Chemical Equilibrium Probed by Two-Dimensional IR Spectroscopy: Hydrogen Bond Dynamics of Methyl Acetate in Water

Marco Candelaresi,[†] Marco Pagliai,[‡] Manuela Lima,[†] and Roberto Righini*[,†,‡]

European Laboratory for Nonlinear Spectroscopy (LENS), Via Nello Carrara 1, and Dipartimento di Chimica, Università di Firenze, Via della Lastruccia 3, 50019 Sesto Fiorentino (Fi), Italy

Received: June 29, 2009; Revised Manuscript Received: September 7, 2009

The solvation dynamics of methyl acetate in heavy water are analyzed by means of two-dimensional infrared spectroscopy, in conjunction with Car−Parrinello molecular dynamics simulations. The C═O stretching infrared band of methyl acetate in water splits into a doublet as a consequence of the hydrogen bond interaction with the solvent, which leads to the equilibrium between two solvated species, consisting of one methyl acetate molecule bonded to one and two water molecules. The structure and dynamics of the water molecules bound to methyl acetate are characterized by means of experiments and simulations, allowing an accurate description of the kinetics of the exchange process and the lifetime of the hydrogen bond.

Introduction

Understanding the structure and dynamics of hydrogen-bonded interactions is of crucial importance in many molecular systems of interest in chemistry, biology, and material science.[1] Two-dimensional nuclear magnetic resonance (2D NMR) spectroscopy has been widely employed for investigating dynamical processes on the microsecond and nanosecond time scales.[2] Techniques such as NOESY and EXSY are of great help in dealing with persistent hydrogen bonds in specific intra- and intermolecular interactions. In many cases, like in solute−solvent interactions, hydrogen bonds are characterized by a very short lifetime, typically in the picosecond or subpicosecond range. Time-resolved optical techniques are definitely better suited than pulsed NMR to address this short time regime. Recently, two-dimensional infrared (2D IR) spectroscopy has been usefully applied for investigating fast dynamics in the liquid phase.[3−13] In cases where the making and breaking of hydrogen bonds correspond to the setup of an equilibrium between well-defined intermolecular structures, subpicosecond 2D IR spectroscopy has been used to gain insight into the underlying fast chemical exchange process.[6−13] In the following we report on the solute−solvent interaction of methyl acetate (MA) in water, investigated and characterized by means of time-resolved nonlinear infrared spectroscopy. The experimental study is accompanied and supported by ab initio Car−Parrinello molecular dynamics (CPMD)[14−17] simulations that are essential in fully characterizing the solvation dynamics of MA.

Experimental and Computational Details

Experimental Details. Methyl acetate (Sigma-Aldrich) is used without further purification. The laser setup consists of a Ti:sapphire oscillator and amplifier system (Thales Laser). The output is a 1 kHz train of 600 μJ pulses at 800 nm with a temporal width of ∼60 fs. Its output is split into equal parts to pump two different optical parametric amplifier (OPA) systems. The pump radiation in this experiment is generated in a traveling wave OPA (TOPAS Light Conversion Ltd.). The probe and reference beams are produced in a homemade OPA. Midinfrared pulses tunable from 3 to 6 μm are obtained by difference-frequency generation of a signal and an idler in a $AgGaS_2$ crystal. In both OPA systems, the infrared output at 6 μm has a spectral width of 200 cm^{-1}, an energy on the order of 1 μJ/pulse, and a pulse duration of ∼100 fs. The pump beam passes through a half-wave plate controlling the polarization and through a variable delay line; its time delay is varied by steps of 25 fs. The probe and reference beams are obtained by reflection from two faces of a wedged CaF_2 plate. Pump, probe, and reference beams are focused into the sample by a parabolic mirror, and the probe and reference beams are then imaged into a flat-field monochromator equipped with a double 32-channel array infrared detector. The pump beam is chopped at half the laser repetition rate, thus eliminating the effects of the long-term laser intensity drift. In narrow band experiments, the pump pulse passes through a Fabry−Perot filter regulated by a feedback-controlled piezoelectric mount. In this configuration the pump has a bandwidth of ∼15 cm^{-1} (fwhm) and a duration of ∼800 fs (fwhm). IR spectra of MA were measured with an FTIR-8400S Shimadzu instrument. The sample consists of a 1 mM solution of MA in D_2O in a CaF_2 cell with a path length of 50 μm. Raman spectra were obtained on a 0.1 M MA water solution using the 514.5 nm line of an Ar^+ laser and a Jobin-Yvon HG25 monochromator equipped with a cooled RCA-C31034A photomultiplier.

Computational Details. We investigate the structure and dynamics of MA with two different computational approaches, for the isolated molecule and small clusters consisting of MA and one or two H-bonded water molecules and for MA in water solutions. The molecular structure and vibrational frequencies of MA were calculated with the Gaussian 03[18] suite of programs adopting the DFT formalism[19,20] using a combination of the BLYP[21,22] or B3LYP[22,23] exchange and correlation functional and the aug-cc-PVTZ basis set. Structure optimizations, with a very tight criterion, and frequency calculations were performed using an improved grid in the numerical evaluation of the integrals (INTEGRAL(GRID═199974)). B3LYP in conjunction with the 6-311++G(d,p) basis set has been revealed to be particularly suitable for the description of H-bonded systems;[24]

* To whom correspondence should be addressed. E-mail: righini@lens.unifi.it.
[†] LENS.
[‡] Dipartimento di Chimica, Università di Firenze.

10.1021/jp906072w CCC: $40.75
Published on Web 09/30/2009

TABLE 1: Salient Structural Parameters for MA[a]

	exptl[28]	MP2/G	B3LYP/G	BLYP/G	BLYP/PW	B3LYP/G*
$r(O-C_c)$	1.360	1.351	1.351	1.371	1.372	1.352
$r(O=C_c)$	1.209	1.212	1.205	1.217	1.220	1.207
$r(O-C_e)$	1.442	1.437	1.437	1.458	1.469	1.440
$r(C_c-C)$	1.496	1.500	1.505	1.516	1.515	1.507
$\angle O=C_c-O$	123.0	123.3	123.3	123.5	122.9	123.2
$\angle C-C_c-O$	111.4	110.8	111.1	110.7	111.1	111.0
$\angle C_c-O-C_e$	116.4	114.1	115.9	115.6	114.6	116.0
$\angle C-C_c=O$	125.6	126.0	125.6	125.8	126.0	125.8

[a] Bond lengths are in angstroms, and bond angles are in degrees. G, G*, and PW refer to calculations with the aug-cc-PVTZ, 6-311++G(d,p), and plane wave basis sets, respectively. C_c and C_e indicate the carbon atoms of the carbonyl and ester groups, respectively.

hence, the geometry optimization and the IR spectra calculations of MA and MA bound to one or two water molecules have been carried out at this level of theory. All the plane wave (PW) based calculations were performed with the CPMD code[25] in conjunction with the BLYP[21,22] exchange and correlation functional, using norm-conserving Martins−Troullier pseudopotentials[26] along with the Kleinman−Bylander[27] decomposition and a plane wave expansion truncated at 70 Ry. Although this computational strategy has been applied with success to study similar systems such as *N*-methylacetamide (NMA), the equilibrium geometry of the isolated MA molecule has been calculated and compared with those from DFT and MP2 with the aug-cc-PVTZ Gaussian basis set. Some structural parameters are reported in Table 1, showing a good agreement between pseudopotentials and all-electron calculations.

The simulations of MA in water solution have been performed using a sample made up by 1 MA and 64 deuterated water molecules in a periodic cubic box with sides of 12.6694 Å (at the experimental density of deuterated water, 1.1056 g·cm^{-3}). The system has been thermalized at 300 K for ∼2.2 ps by velocity scaling. The trajectory has been collected for ∼30 ps (saving the coordinates at each step) with a time step of 5 au (∼0.12 fs) in the NVE ensemble. The fictitius electronic mass was 600 au to allow for an acceptable decoupling between electronic and nuclear degrees of freedom. The average temperature during the simulation was ∼309 ± 15 K.

Results and Discussion

The first helpful information to characterize the interactions between MA and water can be obtained from infrared spectroscopy. The IR spectra of MA in CCl_4, in CH_3CN, and in water in the region of the C═O stretching mode are reported in Figure 1. The absorption band shows a marked dependence on the nature of the solvent, namely, on its polarity and capability of forming H-bonds. In CCl_4 (Figure 1a) and CH_3CN (Figure 1b) only one single peak at 1747 and 1741 cm^{-1}, respectively, is present, whereas in D_2O (Figure 1c) the C═O band splits into a doublet and is shifted to lower frequency. The band is noticeably narrower in CCl_4, as a consequence of the much smaller electrostatic solute−solvent interactions that take place in that solvent. The two peaks are centered at 1703 and 1727 cm^{-1}. In view of the large effect of the solute−solvent interaction on the absorption frequency (the gas-phase transition is at 1770 cm^{-1}), the splitting into a doublet in water suggests the existence of two different species in solution.

That an equilibrium is responsible for the observed spectral feature is demonstrated by the temperature dependence of the band shape in water. Figure 2 shows the FTIR spectrum in D_2O at different temperatures: the relative intensities of the two bands

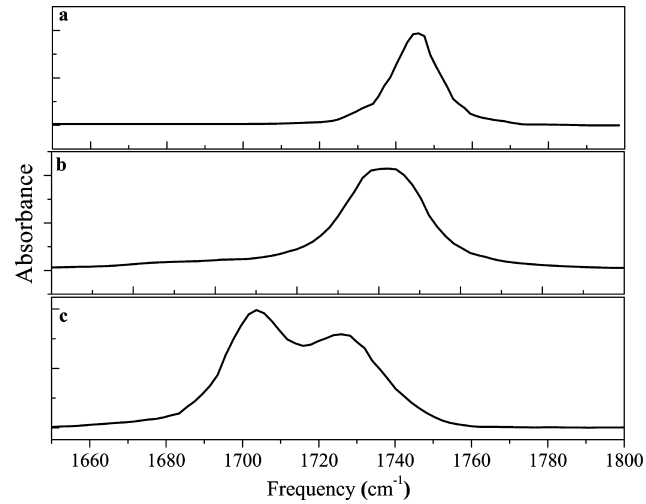

Figure 1. FTIR spectra of MA at room temperature in (a) CCl_4, (b) CH_3CN, and (c) D_2O.

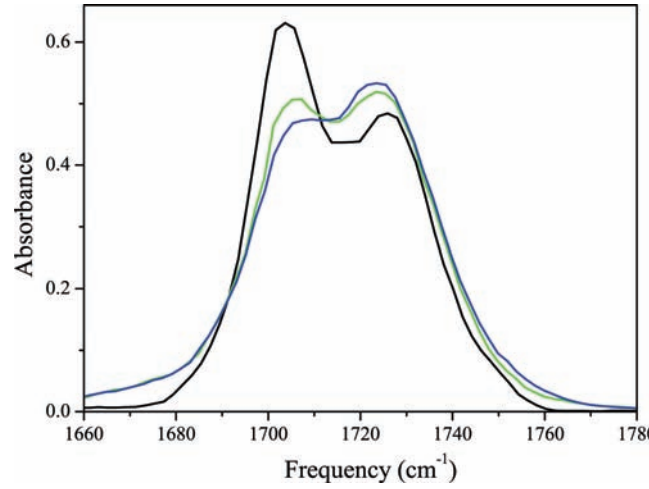

Figure 2. FTIR spectra of MA in D_2O as a function of temperature: black, T = 280 K; green, T = 323 K; blue, T = 338 K.

change in the temperature range between 280 and 338 K. At 323 K the spectrum exhibits two bands with equal intensity. At high temperature the more intense band is that at higher frequencies, whereas at low temperature the opposite occurs.

As a possible explanation of this behavior, one may consider that ester molecules can adopt either the *Z* or the *E* conformation and that the nature of the solvent has a strong influence on this equilibrium.[28] The *Z-trans* conformation is the most stable for the isolated molecule. Water reduces the free energy difference between the two MA conformers from 7.6 kcal/mol in the gas phase to 3.2 ± 0.5 kcal/mol in water solution.[29] This relative stabilization is attributed to the H-bond interaction between the solvent and the oxygen atoms of MA. In principle then, the doublet observed in water for the C═O band could be attributed to the coexistence of the two MA conformers.

Although the *E* conformer is more stabilized than the *Z* conformer in solvents with a high dielectric constant,[28−31] the *Z*−*E* interconversion requires the crossing of a free energy barrier of 10.5 kcal/mol, which makes the presence in solution of the *E* conformer highly unlikely. The Raman spectrum between 500 and 1800 cm^{-1}, shown in Figure 3, is very useful to determine the nature of the MA conformers present in the aqueous solution. According to previous assignments,[32,33] the bands between 600 and 900 cm^{-1}, and in particular the bands at 844 and 638 cm^{-1},[32] corresponding to CH_3-O stretching and

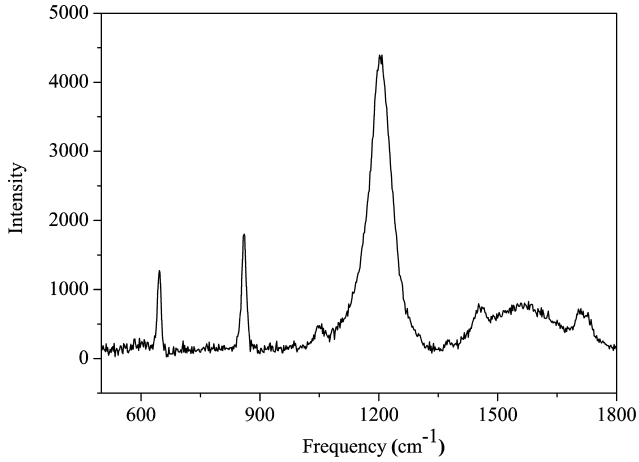

Figure 3. Raman spectrum of MA in D_2O at room temperature.

skeletal normal modes, are characteristic of the *Z* conformer of MA and support the conclusion of George et al.[32] that the *Z* conformer is the only species present in solution. As stated in ref 33, these results are confirmed also by dipole moment,[34] electron diffraction,[35] microwave,[36] and IR[37,38] measurements.

We can then rule out the possibility that *Z*−*E* equilibrium is responsible for the double peak characterizing the C═O band of MA in water. Thus, we attribute this spectral feature to the setup of an equilibrium between two local structures involving specific interactions between MA and the water molecules; it is an obvious conclusion that the equilibrium involves two different hydrogen-bonded water−MA complexes. The behavior in fact is similar to that reported for MA in methanol.[39] In that paper the appearance of two distinct spectral components was attributed to the coexistence of single-bonded and free MA, while the double-bonded species contribute with a very weak shoulder on the low-frequency side of the C═O stretching band. Additional support to this hypothesis comes from the somehow similar behavior observed for the amide I mode of NMA in methanol,[10,40−42] where the equilibrium between two different solvation structures is responsible for the band shape of the C═O stretching vibration. The solvation dynamics of NMA in water and methanol solutions have been studied by several groups by means of classical molecular dynamics simulations.[40−47] However, Iuchi et al.[42] and Yang et al.[45] demonstrated the importance of including polarization effects to properly describe the hydrogen bond dynamics and the IR spectra. In particular, Yang et al.,[45] adopting a QM/MM method, observed a strong intramolecular charge reorganization, with an increase of the dipole moment of NMA from 3.51 D in the gas phase to 7.56 D in solution. A similar result was obtained in CPMD simulations,[48] where the dipole moment changes from 3.99 to 6.96 D.

To account for the large charge reorganization characterizing the H-bonded solute−solvent interaction, we performed an ab initio simulation of an MA aqueous solution, using the Car−Parrinello[14−17] approach. In Figure 4a we show the pair radial distribution functions for the interactions of a water hydrogen atom with the carbonyl and ester oxygens. It is evident that MA interacts with the solvent prevalently through its carbonyl oxygen, whereas the ester oxygen atom forms only extremely weak H-bonds. In the following analysis then, we will consider only carbonyl oxygen−water interactions. Figure 4b shows the angular distribution function limited to water molecules H-bonded to the C═O group. It can be seen that for H-bond distances lower than 2.5 Å the ∠H−O···O angle is definitively less than 40°, as expected for this type of system.[49−51]

Our results indicate that MA forms strong hydrogen bonds with water, similarly to the finding of recent calculations for NMA, where a similar computational approach was adopted.[48] However, the number of water molecules H-bonded to MA is definitely smaller: the coordination number in fact is 1.3 for MA and 2.0 for NMA. We can then suppose that the double peak structure of the C═O band in MA can be explained as due to the rapid interchange between configurations where the carbonyl is hydrogen bonded to one and to two water molecules. The same spectral feature would not be visible in NMA, whose C═O group is always bonded to two water molecules. A first confirmation of this picture comes from the ab initio calculation made for two model systems consisting of an MA molecule bonded to one and to two water molecules. In fact, DFT calculations at the B3LYP/6-311++G(d,p) level show that the single-bonded and the double-bonded MA−water complexes have different C═O stretching frequencies, with a frequency separation (see Figure 5) very close to the one measured in the FTIR spectra of MA. Setting to 1 the intensity for the double-H-bonded complex, the calculated intensities for the two possible single-bonded configurations (differing for the localization of the hydrogen bond) have very close values 0.87 and 0.92, as shown in Figure 5.

The ab initio calculations then confirm the attribution of the peaks at 1703 and 1727 cm^{-1} to the interaction of MA with two water molecules and one water molecule, respectively, and represent the starting point for the interpretation of the experimental findings. We already have mentioned that time-resolved two-dimensional infrared spectroscopy has been successfully used to characterize the fast chemical exchange process between molecular species. The basic point is that the two species A and B are characterized by different IR resonance frequencies, ν_A and ν_B: in a 2D IR spectrum the two absorptions will appear as diagonal resonances. For an excitation pulse resonant with the absorption of the A species, at zero delay time the probe pulse measures a diagonal resonance at ν_A. As time goes on, due to the A → B process, an increasing fraction of the initially excited A molecules transform into B species, and an off-diagonal peak is observed in the two-dimensional spectrum in correspondence with the pump frequency ν_A and the probe frequency ν_B. This simple population exchange picture is valid provided that the exchange is slow in comparison to the dephasing rate of the two states. In fact, as shown by Kim and Hochstrasser,[8] if the exchange happens on a time scale shorter than the coherence time, coherence is transferred back and forth between the A and B states, resulting in a broadening and coalescing of the two FTIR resonances into a single band. Correspondingly, off-diagonal peaks can be observed in the 2D IR spectrum. These nonlinear spectral features due to coherence transfer are observed at zero delay time: the intensity growth of the cross peaks with increasing delay is instead due to the population exchange. In the hypothesis that the FTIR doublet can be attributed to the chemical exchange between MA−2D_2O (double-bonded, A species) and MA−D_2O (single-bonded, B species) solvation complexes, the population exchange picture applies exactly to our case, with ν_A = 1703 cm^{-1} and ν_B = 1727 cm^{-1}. In fact, the 2D spectra in Figure 6 show strong off-diagonal peaks whose intensities, relative to those of the diagonal resonance, increase with the time delay. This is better seen by taking horizontal slices of the 2D spectra of Figure 6 at different delay times. In Figure 7 slices corresponding to excitation on the red and blue tails of the band are shown; the intensities of the spectra at different time delays have been normalized to

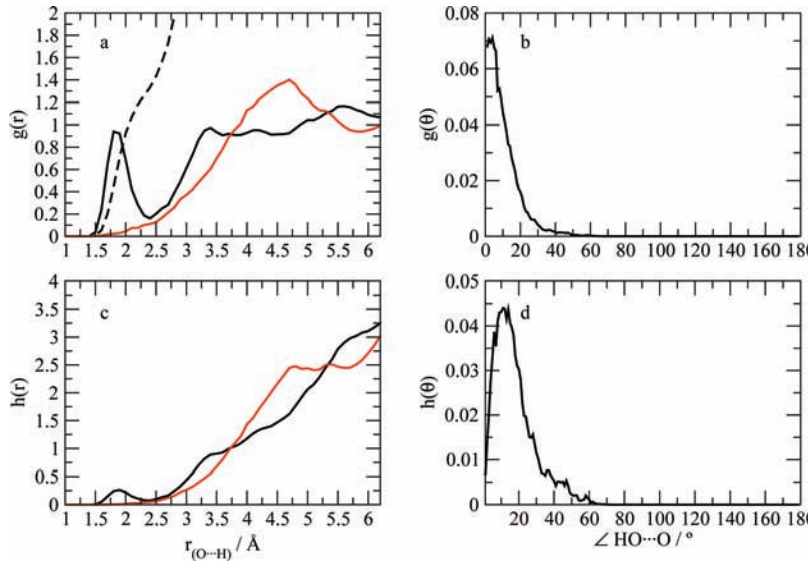

Figure 4. (a) Pair radial distribution function (full black line) and integration number (dashed black line) for the carbonyl oxygen−D_2O interaction. The red line refers to the ester oxygen−D_2O interaction. (b) Angular distribution function of the D_2O molecule H-bonded with MA. (c, d) Unnormalized pair radial and angular distribution functions, respectively.

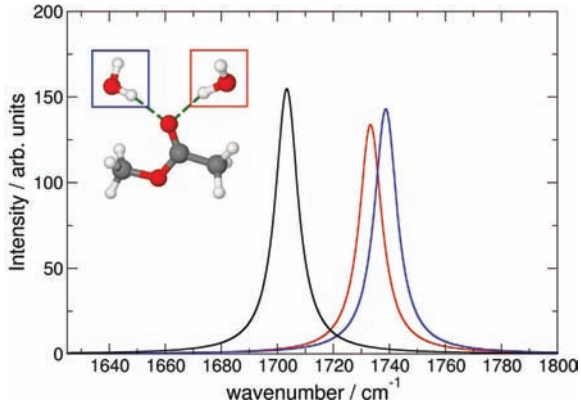

Figure 5. Calculated IR spectrum of MA in the C═O region. The black line refers to the double-H-bonded MA−water complex. The blue line and the red line refer to the single-H-bonded complexes, taking into consideration only the molecule indicated in the inset. The vibrational frequencies have been obtained on the equilibrium structures.

the diagonal peak intensity, so that the increasing relative amplitude of the off-diagonal peaks is made evident.

The exchange between species A and B

$$\begin{aligned} A &\xrightarrow{k_1} B \\ B &\xrightarrow{k_2} A \end{aligned} \tag{1}$$

is described by first-order kinetic equations, whose solution is

$$N_A(t) = 1 - N_B(t) = \frac{k_1}{k_1 + k_2}\{1 - \exp[-(k_1 + k_2)t]\} \tag{2}$$

where $N_A(t)$ and $N_B(t)$ are the fractions of double-bonded and single-bonded species, respectively. For $t \rightarrow \infty$ the ratio of N_A and N_B is the equilibrium constant for the exchange process, which, in turn, equals the ratio between the kinetic constants:

$$K = \frac{N_A^{\infty}}{N_B^{\infty}} = \frac{k_2}{k_1} \tag{3}$$

The non-linear spectra recorded at different delay times (see Figures 6 and 7) show no evidence of inhomogeneous broadening, and also the line widths are practically constant in time. Spectral diffusion is actually expected to be very fast in a fast solvent such as water, and it is evidently completed within the duration of the excitation pulse. With good approximation we can then consider the line shapes of the diagonal and off-diagonal peaks constant throughout the experimental time window, with a remarkable simplification of the data analysis.[40,41,52] However, the off-diagonal peak intensities obtained from the measured spectral evolution need some treatment before being used for evaluating the kinetic constants. The first point to be considered is that the growth of these peaks is accompanied by the overall signal decrease due to the population decay of the C═O excited state. To correct our data for this effect, we have measured with a broad-band pump−probe experiment the vibrational lifetime of the MA C═O stretch in water, obtaining the value $\tau_v = 900 \pm 20$ fs. The experiment shows no detectable difference in the decay of the two spectral components: the same lifetime is then assumed for both vibrational states. We then correct our data for the effect of the population relaxation, by dividing the measured time evolution of the peak intensities by a normalized exponential function with a decay time constant of 900 fs. Second, we have to take into account that when the pump is centered at, say, ω_A, the resonance at ω_B can also be directly excited, to some minor extent, by the spectral tail of the Lorentzian pump pulse. This leads to a constant in time (once the lifetime correction has been introduced) contribution to the off-diagonal signal. This constant term is easily identified and subtracted from the measured kinetic traces. Finally, the temporal width of the excitation and probe pulses must be considered: the time domain instrumental function is obtained

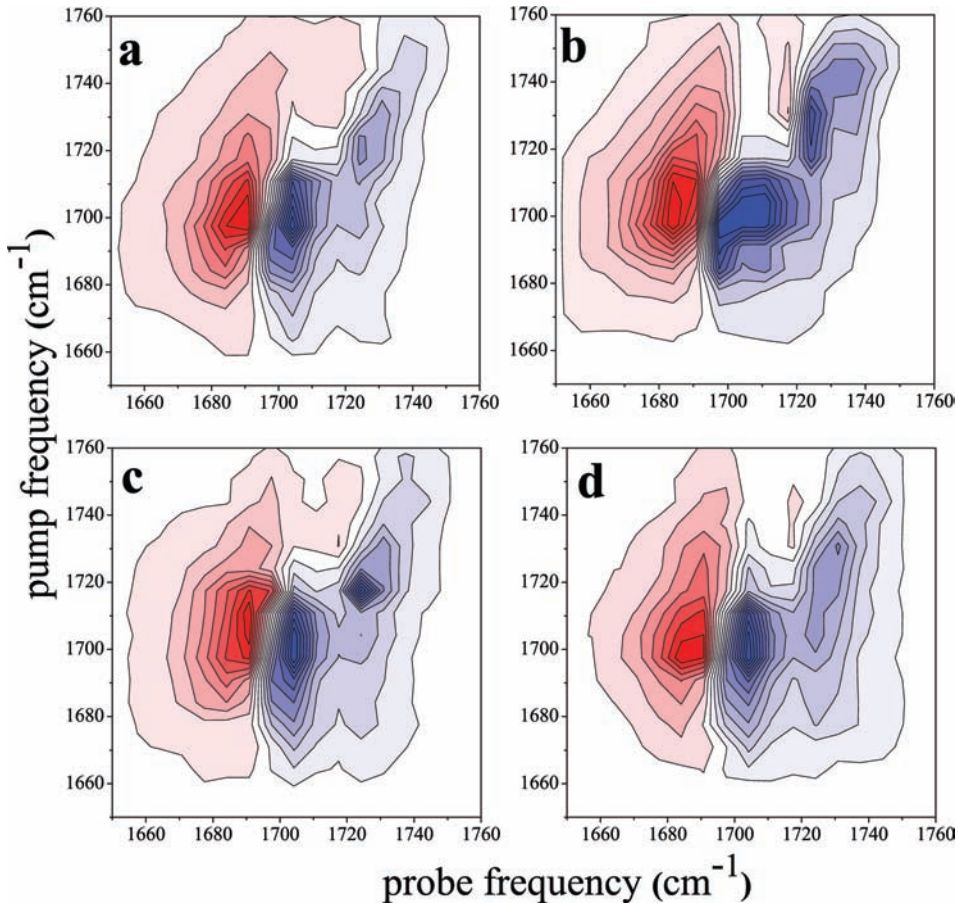

Figure 6. 2D IR spectra of MA in D_2O: (a, c) spectra recorded at 0 and 700 fs, respectively, in parallel polarization, (b, d) spectra recorded at the same delay in perpendicular polarization.

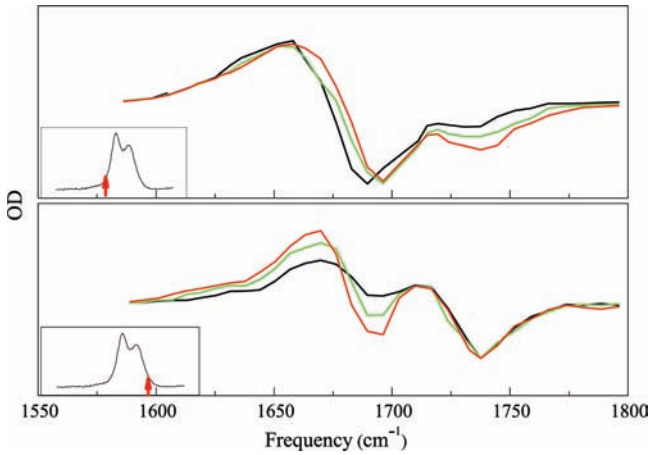

Figure 7. Single-wavelength pump experiment: top, 1688 cm^{-1}; bottom, 1744 cm^{-1}; black line, 0.26 ps; green line, 1.00 ps; red line, 1.50 ps.

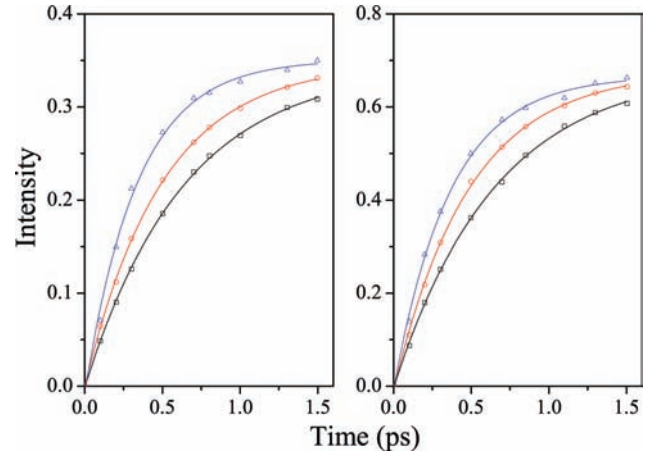

Figure 8. Growth of the off-diagonal peak intensity (left, 1688 cm^{-1}; right, 1744 cm^{-1}) at 280 K (black line), 293 K (red line), and 313 K (blue line).

by convoluting the short (100 fs) Gaussian probe pulse with the Fourier transform of the Lorentzian (17 ± 1 cm^{-1} fwhm) pump pulse passing through the Fabry−Perot filter. Thus, we obtain the "true" time evolution of the cross peak intensities from the experimental data by deconvolution. The bandwidth of the pump pulse and its relatively long time duration are also responsible for the appearance of cross peaks at zero delay time. Of course we cannot exclude that some contribution from coherence transfer processes[8] is present; however, our experimental conditions do not allow any conclusion on this point to be drawn.

TABLE 2: Exponential Fit Results of the Data in Figure 8 at Different Temperatures

T (K)	$\tau = 1/(k_1 + k_2)$ (ps)
280	0.65 ± 0.06
293	0.50 ± 0.09
313	0.35 ± 0.12

The time evolution of the off-diagonal peaks at 1688 and 1744 cm^{-1} measured at 280, 293, and 313 K is reported in Figure 8. The corresponding time constants obtained by an exponential fit using eq 2 are collected in Table 2.

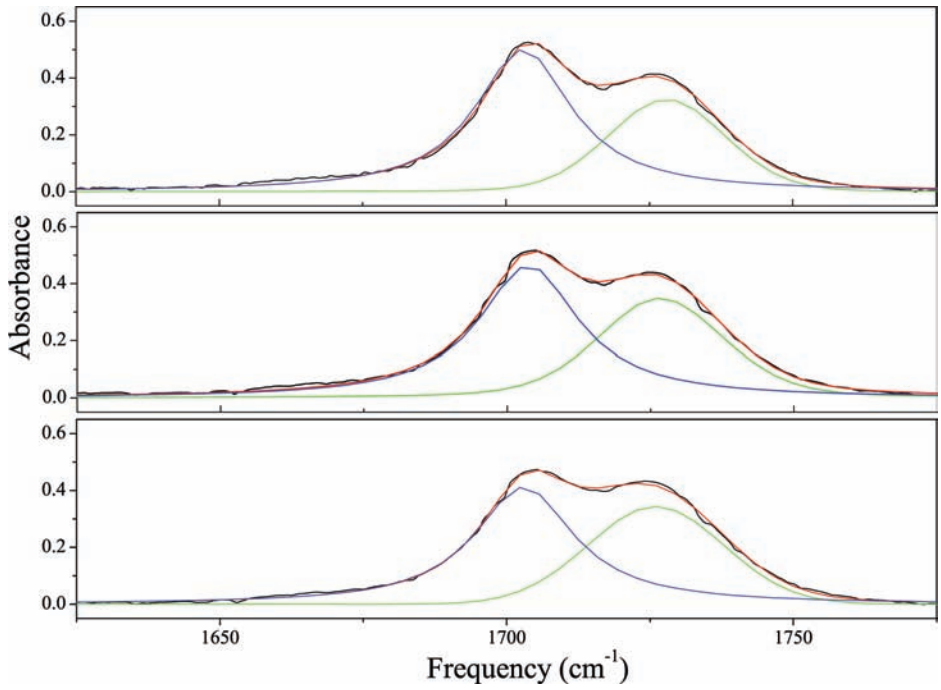

Figure 9. Fits of the FTIR spectrum in the C═O stretching region at different temperatures: from top to bottom, 280, 293, and 313 K, respectively; black curve, experimental spectrum; red line, fit spectrum; blue line, Lorentzian curve; green line, Voight curve. The χ^2 values for the fits of the three spectra at increasing temperature are 6.5×10^{-5}, 3.9×10^{-5}, and 5.7×10^{-5}, respectively.

TABLE 3: Value of the Equilibrium Constant, $K = N_A^\infty/N_B^\infty$, and of the Kinetic Constants for Breaking (k_1) and Making (k_2) H-Bonds at Different Temperatures

T (K)	K	k_1 (s^{-1})	k_2 (s^{-1})
280	1.534	$(6.1 \pm 0.2) \times 10^{11}$	$(9.3 \pm 0.3) \times 10^{11}$
293	1.196	$(9.1 \pm 0.1) \times 10^{11}$	$(10.9 \pm 0.2) \times 10^{11}$
313	1.112	$(13.5 \pm 0.6) \times 10^{11}$	$(15.0 \pm 0.7) \times 10^{11}$

The populations of the A and B species which appear in the equilibrium constant of eq 3 are obtained directly from the experimental FTIR spectra. As shown in Figure 9, the two spectral components contributing to the absorption band are obtained by decomposition adopting Voight profiles. Actually, the low-frequency band, corresponding to the absorption of the double-bonded species, is well fitted by an almost pure Lorentzian line shape. The broader line width of the high-frequency component is possibly related to the two possible geometries of the single-bonded species, as predicted by the calculations of Figure 5. Taking into account the IR intensities predicted for the two species by ab initio calculations (1 and 0.89 for A and B, respectively; see Figure 5), the N_A^∞/N_B^∞ ratio is obtained directly from the relative intensities of the two spectral components.

From the equilibrium constants evaluated at the different temperatures and from the values of $k_1 + k_2$ given in Table 2, using eq 3, we finally obtain the kinetic constants for the exchange of single-bonded and double-bonded species. Their values are collected in Table 3. The activation energies (E_a) for the two processes are calculated from an Arrhenius plot of the temperature dependence of the kinetic constants of Table 3; we obtain $E_a = 4.2 \pm 0.6$ kcal/mol for the breaking of one H-bond of the double-bonded species and $E_a = 2.1 \pm 0.6$ kcal/mol for the making of the second H-bond.

A more detailed description of the structure and dynamics of the solvation shell is predicted by the results of CPMD simulations. The H-bond configurational space is conveniently analyzed by means of the pair radial and angular distribution

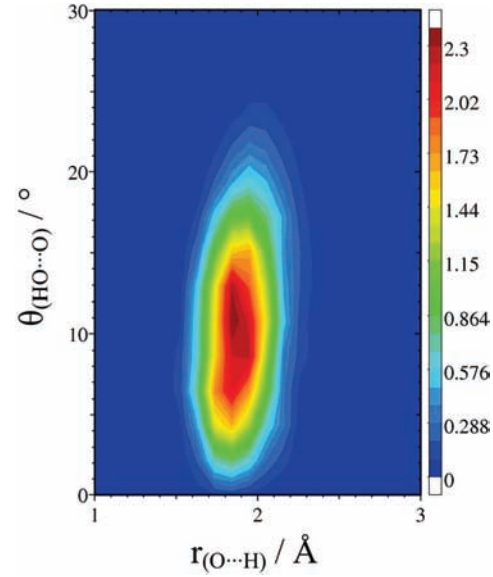

Figure 10. H-bond configuration space obtained as the weighted $g(r,\theta)$ function from eq 4.

function, $g(r,\theta)$, weighted by the recently introduced[51,53−55] function

$$F_j^{HB} = A(r(t))\, B(\theta(t)) \tag{4}$$

$A(r(t))$ and $B(\theta(t))$ are given by

$$\begin{cases} A(r(t)) = \exp[-(r_e - r_j(t))^2/(2\sigma_r^2)] & \text{if } (r_e - r_j(t)) < 0 \\ A(r(t)) = 1 & \text{if } (r_e - r_j(t)) \geq 0 \\ B(\theta(t)) = \exp[-(\theta_e - \theta_j(t))^2/(2\sigma_\theta^2)] & \text{if } (\theta_e - \theta_j(t)) < 0 \\ B(\theta(t)) = 1 & \text{if } (\theta_e - \theta_j(t)) \geq 0 \end{cases} \tag{5}$$

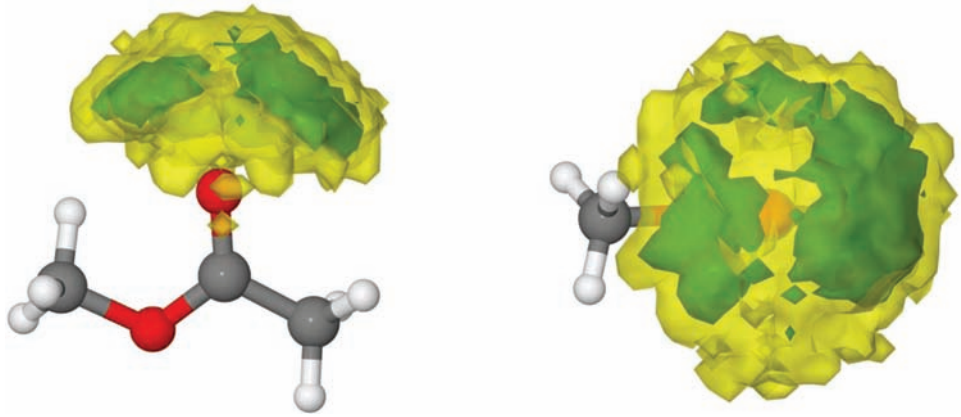

Figure 11. SDF along two different views of the H-bonded water molecules around the carbonyl oxygen atom of MA. Green and yellow isosurfaces refer to 70% and 99% probability of finding a H-bond, respectively.

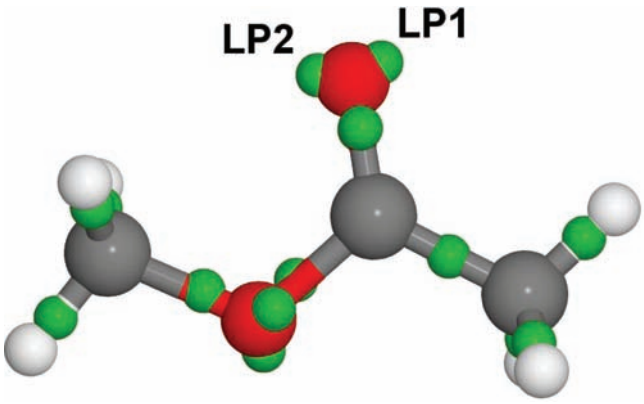

Figure 12. Molecular structure of MA. The green spheres indicate the position of the WFCs (electron pairs).

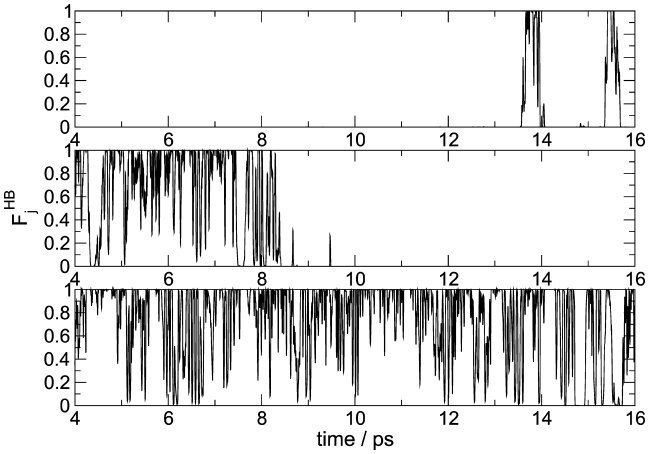

Figure 13. Evolution of F_j^{HB} for the molecules with $j = 38$ (upper panel), 30 (central panel), and 47 (lower panel) in the temporal window between 4 and 16 ps of the entire CPMD simulation.

The values of the parameters r_e, θ_e, σ_r and σ_θ are directly extracted from the un-normalized pair radial, $h(r)$, and angular, $h(\theta)$, distribution functions (see Figure 4c,d). In the above definitions, r_e is the position of the first peak in $h(r)$ and θ_e is the position of the first peak in $h(\theta)$, whereas σ_r and σ_θ are the half-widths at half-maximum in $h(r)$ and $h(\theta)$, respectively. From eq 4, we obtain the percentages of water molecules involved in 0, 1, 2, and 3 H-bonds with MA; they are 4.1%, 54.0%, 40.6%, and 1.3%, respectively; as already noticed, these values refer to a simulation temperature of 309 K. The surface spanned by the H-bond, reported in Figure 10, shows a maximum for the $r(O\cdots H)$ distance of about 1.9 Å and for the $\theta(HO\cdots O)$ angle of about 10°, indicating a rather strong interaction, although weaker than previously found for NMA.[42,48]

The reorganization of the solvent around the carbonyl oxygen atom is described by the spatial distribution function (SDF) given in Figure 11. The green and yellow isosurfaces refer to 70% and 99% probability, respectively, of finding a water molecule H-bonded to MA. As observed for NMA,[56] the high mobility of the water molecules around the carbonyl oxygen atom determines a surface close to a hemisphere. However, for the 70% probability isosurface, the distribution is not uniform: two distinct high-density regions can be clearly identified.

From the analysis of the electronic structure of MA in terms of maximally localized Wannier function centers (WFCs) indicated in Figure 12, this spatial arrangement corresponds to the interaction with the lone pairs on the carbonyl oxygen. The presence of two electron pairs (LP1 and LP2 in Figure 12) on the carbonyl oxygen atom allows for the formation of up to two H-bonds. It is possible to note from the extent of the surface that the interactions between the lone pairs and the solvent are not equivalent. In fact, the region spanned by the H-bond water molecules close to the LP1 region shows a higher probability density than that of LP2. The analysis of the variation of the lone pair−oxygen distance during the simulation run shows that the LP1−oxygen distance is on average larger than that of LP2, being up to 0.05 Å higher than the equilibrium value. In fact, the polarization effects are large and cause an increase of the dipole moment of MA from ∼1.93 D for the isolated molecule to ∼3.27 D in the bulk phase. A similar effect was observed for NMA.[42,45,48] The dipole moment of MA can be directly related to the number of H-bonds formed with the solvent: the average dipole moment of MA bound to one water molecule is 3.15 D, whereas if MA interacts with two molecules, the average dipole moment increases to 3.55 D. It is interesting to note that the average dipole moment of the molecule that is not H-bonded with the solvent is 2.19 D, a value very close to that found for the isolated molecule.

According to Haughney et al.,[57] the H-bond lifetime can be calculated from the expression

$$\tau_{HB} = \sum_{n=0}^{\infty} \frac{1}{2}\Delta t[H(t_n) + H(t_{n+1})] \qquad (6)$$

where

$$H(\tau_m) = \sum_{n=m}^{\infty} N(t_{n+1}) / \sum_{n=1}^{\infty} N(t_n)\, H(0) = 1 \qquad (7)$$

and $N(t_n)$ is a histogram containing the probability that a given H-bond survives at time t_n.

Figure 13 shows the time evolution function of the F_j^{HB} function, as defined by eq 4, for three water molecules (labeled with $j = 30$, 38, and 47) which interact with MA, in the temporal window between 4 and 16 ps of the CPMD simulation. Although the water molecule with $j = 47$ (lower panel) interacts with the solute during the entire temporal range, it is evident that H-bonds are broken and formed continuously. A similar behavior occurs for the second water molecule H-bonded with MA, although for a shorter temporal interval, as reported in the central and upper panels for the molecules with $j = 38$ and 30, respectively. This continuous breaking and forming determines the short average H-bond lifetime (~0.34 ps) obtained from the entire simulation.

Conclusions

The 2D IR pump probe techniques can be used to fully characterize the solvation dynamics of MA in D_2O solution. The available time resolution allows the fast making and breaking of hydrogen bonds between MA and water molecules to be probed. The 2D spectra provide an explanation of the line shape of the FTIR spectrum. In fact, the off-diagonal peaks that appear in 2D spectra are the signature of the solute−solvent dynamics not accessible by FTIR and Raman spectra. In this case the cross peaks are due to the making and breaking of hydrogen bonds between water and MA, corresponding to equilibrium between double-bonded and single-bonded species. Car−Parrinello simulations confirm this interpretation, providing an average lifetime of the H-bond of 0.34 ps. CPMD simulations also show that one of the two lone pairs provides a more flexible docking point for water molecules.

Acknowledgment. This work was supported by the Ministero dell'Istruzione, dell'Università e della Ricerca (MIUR), and by Ente Cassa di Risparmio di Firenze. We thank Dr. Maurizio Muniz-Miranda for help with the experimental measurements of the methyl acetate Raman spectra.

References and Notes

(1) Krimm, S.; Bandekar, J. *Adv. Protein Chem.* **1986**, *38*, 181.
(2) Ernst, R. R.; Bodenhausen, G.; Wokaun, A. *Principles of Nuclear Magnetic Resonance in One and Two Dimensions*; Oxford University Press: Oxford, U.K., 1987.
(3) Cho, M. *Chem. Rev.* **2008**, *109*, 1331.
(4) Zhuang, W.; Hayashi, T.; Mukamel, S. *Angew. Chem., Int. Ed.* **2009**, *48*, 3750.
(5) Kim, Y. S.; Hochstrasser, R. M. *J. Phys. Chem. B* **2009**, *113*, 8321.
(6) Hamm, P.; Lim, M.; Hochtrasser, R. M. *J. Phys. Chem. B* **1998**, *102*, 6123.
(7) Kim, Y. S.; Hochstrasser, R. M. *Proc. Natl. Acad. Sci. U.S.A.* **2005**, *102*, 11185.
(8) Kim, Y. S.; Hochstrasser, R. M. *J. Phys. Chem. B* **2006**, *110*, 8531.
(9) Zheng, J.; Kwak, K.; Asbury, J.; Chen, X.; Piletic, I. R.; Fayer, M. D. *Science* **2005**, *309*, 1338.
(10) Woutersen, S.; Mu, Y.; Stock, G.; Hamm, P. *Chem. Phys.* **2001**, *266*, 137.
(11) Kim, Y. S.; Hochstrasser, R. M. *J. Phys. Chem. B* **2007**, *111*, 9697.
(12) Ghosh, A.; Remorino, A.; Tucker, M. J.; Hochstrasser, R. M. *Chem. Phys. Lett.* **2009**, *469*, 325.
(13) Bagchi, S.; Charnley, A. K.; Smith, A. B., III; Hochstrasser, R. M. *J. Phys. Chem. B* **2009**, *113*, 8412.
(14) Car, R.; Parrinello, M. *Phys. Rev. Lett.* **1985**, *55*, 2471.
(15) Parrinello, M. *Solid State Commun.* **1997**, *102*, 107.
(16) Parrinello, M. *Comput. Sci. Eng.* **2000**, *2*, 22.
(17) Tse, J. S. *Annu. Rev. Phys. Chem.* **2002**, *53*, 249.
(18) Frisch, M. J.; Trucks, G. W.; Schlegel, H. B.; Scuseria, G. E.; Robb, M. A.; Cheeseman, J. R.; Montgomery, Jr., J. A.; Vreven, T.; Kudin, K. N.; Burant, J. C.; Millam, J. M.; Iyengar, S. S.; Tomasi, J.; Barone, V.; Mennucci, B.; Cossi, M.; Scalmani, G.; Rega, N.; Petersson, G. A.; Nakatsuji, H.; Hada, M.; Ehara, M.; Toyota, K.; Fukuda, R.; Hasegawa, J.; Ishida, M.; Nakajima, T.; Honda, Y.; Kitao, O.; Nakai, H.; Klene, M.; Li, X.; Knox, J. E.; Hratchian, H. P.; Cross, J. B.; Adamo, C.; Jaramillo, J.; Gomperts, R.; Stratmann, R. E.; Yazyev, O.; Austin, A. J.; Cammi, R.; Pomelli, C.; Ochterski, J. W.; Ayala, P. Y.; Morokuma, K.; Voth, G. A.; Salvador, P.; Dannenberg, J. J.; Zakrzewski, V. G.; Dapprich, S.; Daniels, A. D.; Strain, M. C.; Farkas, O.; Malick, D. K.; Rabuck, A. D.; Raghavachari, K.; Foresman, J. B.; Ortiz, J. V.; Cui, Q.; Baboul, A. G.; Clifford, S.; Cioslowski, J.; Stefanov, B. B.; Liu, G.; Liashenko, A.; Piskorz, P.; Komaromi, I.; Martin, R. L.; Fox, D. J.; Keith, T.; Al-Laham, M. A.; Peng, C. Y.; Nanayakkara, A.; Challacombe, M.; Gill, P. M. W.; Johnson, B.; Chen, W.; Wong, M. W.; Gonzalez, C.; Pople, J. A. *Gaussian 03*, revision C.02; Gaussian, Inc.: Wallingford, CT, 2004.
(19) Kohn, W.; Sham, L. J. *Phys. Rev.* **1965**, *140*, A1133.
(20) Hohenberg, P.; Kohn, W. *Phys. Rev.* **1964**, *136*, B864.
(21) Becke, A. D. *Phys. Rev. A* **1988**, *38*, 3098.
(22) Lee, C.; Yang, W.; Parr, R. G. *Phys. Rev. B* **1988**, *37*, 785.
(23) Becke, A. D. *J. Chem. Phys.* **1993**, *98*, 5648.
(24) Rabuck, A. D.; Scuseria, G. E. *Theor. Chem. Acc.* **2000**, *104*, 439.
(25) Calculations used the CPMD code (http://www.cpmd.org/). Copyright IBM Corp. 1990−2008. Copyright MPI für Festkörperforschung, Stuttgart, Germany, 1997−2001.
(26) Troullier, N.; Martins, J. L. *Phys. Rev. B* **1991**, *43*, 1993.
(27) Kleinman, L.; Bylander, D. M. *Phys. Rev. Lett.* **1982**, *48*, 1425.
(28) Allinger, N. L.; Zhu, Z. S.; Chen, K. *J. Am. Chem. Soc.* **1992**, *114*, 6120.
(29) Wiberg, K. B.; Wong, M. W. *J. Am. Chem. Soc.* **1993**, *115*, 1078.
(30) Byun, K.; Mo, Y.; Gao, J. *J. Am. Chem. Soc.* **2001**, *123*, 3974.
(31) Evanseck, J. D.; Houk, K. N.; Briggs, J. M.; Jorgensen, W. L. *J. Am. Chem. Soc.* **1994**, *116*, 10630.
(32) George, W. O.; Houston, T. E.; Harris, W. *Spectrochim. Acta, A* **1974**, *30*, 1035.
(33) George, W. O.; Hassid, D. V.; Maddams, W. F. *J. Chem. Soc., Perkin Trans. 2* **1972**, 1029.
(34) Marsden, R. J. B.; Sutton, L. E. *J. Chem. Soc.* **1936**, 1383.
(35) O'Gorman, J.; Shand, W.; Schomaker, V. *J. Am. Chem. Soc.* **1950**, *72*, 4222.
(36) Curl, R. F. *J. Chem. Phys.* **1959**, *30*, 1529.
(37) Wilmshurst, J. K. *J. Mol. Spectrosc.* **1959**, *1*, 201.
(38) Oki, M.; Nakanishi, H. *Bull. Chem. Soc. Jpn.* **1970**, *43*, 2558.
(39) Banno, M.; Ohta, K.; Tominaga, K. *J. Raman Spectrosc.* **2008**, *39*, 1531.
(40) Kwac, K.; Lee, H.; Cho, M. *J. Chem. Phys.* **2004**, *120*, 1477.
(41) Kwac, K.; Cho, M. *J. Raman Spectrosc.* **2005**, *36*, 326.
(42) Iuchi, S.; Morita, A.; Kato, S. *J. Phys. Chem. B* **2002**, *106*, 3466.
(43) Kwac, K.; Cho, M. *J. Chem. Phys.* **2003**, *119*, 2247.
(44) Schmidt, J. R.; Corcelli, S. A.; Skinner, J. L. *J. Chem. Phys.* **2004**, *121*, 8887.
(45) Yang, S.; Cho, M. *J. Chem. Phys.* **2005**, *123*, 134503.
(46) DeCamp, M. F.; DeFlores, L.; McCracken, J. M.; Tokmakoff, A.; Kwac, K.; Cho, M. *J. Phys. Chem. B* **2005**, *109*, 11016.
(47) Hayashi, T.; Mukamel, S. *J. Chem. Phys.* **2006**, *125*, 194510.
(48) Gaigeot, M. P.; Vuillemier, R.; Sprik, M.; Borgis, D. *J. Chem. Theory Comput.* **2005**, *1*, 722.
(49) Desiraju, G. R.; Steiner, T. *The Weak Hydrogen Bond*; Oxford University Press: Oxford, U.K., 1999.
(50) Luzar, A.; Chandler, D. *Phys. Rev. Lett.* **1996**, *76*, 928.
(51) Pagliai, M.; Cardini, G.; Righini, R.; Schettino, V. *J. Chem. Phys.* **2003**, *119*, 6655.
(52) Šanda, F.; Mukamel, S. *J. Chem. Phys.* **2006**, *125*, 014507.
(53) Pagliai, M.; Cardini, G.; Schettino, V. *J. Phys. Chem. B* **2005**, *109*, 7475.
(54) Faralli, C.; Pagliai, M.; Cardini, G.; Schettino, V. *J. Phys. Chem. B* **2006**, *110*, 14923.
(55) Pagliai, M.; Bellucci, L.; Muniz-Miranda, M.; Cardini, G.; Schettino, V. *Phys. Chem. Chem. Phys.* **2006**, *8*, 171.
(56) Mantz, Y. A.; Gerard, H.; Iftimie, R.; Martyna, G. J. *J. Phys. Chem. B* **2006**, *110*, 13523.
(57) Haughney, M.; Ferrario, M.; McDonald, I. R. *J. Phys. Chem.* **1987**, *91*, 4934.

JP906072W